

Theoretical study of ternary silver fluorides AgMF_4 ($\text{M} = \text{Co}, \text{Ni}, \text{Cu}$) formation at pressures up to 20 GPa

M.A. Domański^{1*}, M. Derzsi^{1,2} and W. Grochala^{1*}

¹Centre of New Technologies, University of Warsaw, S. Banacha 2C, 02-097 Warsaw, Poland

²Advanced Technologies Research Institute, Faculty of Materials Science and Technology in Trnava,
Slovak University of Technology in Bratislava, 917 24, Trnava, Slovakia

Keywords: theoretical modelling, silver fluorides, magnetic ordering, crystal structure prediction

*e-mail: m.domanski@cent.uw.edu.pl, w.grochala@cent.uw.edu.pl

This work is dedicated to Prof. Gary Schrobilgen at his 75th birthday

Abstract

Only several compounds bearing Ag(II) cation and other transition metal cation have been known. Herein, we predict stability and crystal structures of hypothetical ternary silver(II) fluorides with copper, nickel and cobalt in 1:1 stoichiometry at pressure range from 0 GPa up to 20 GPa within the frame of Density Functional Theory. Calculations show that AgCoF_4 could be synthesized already at ambient conditions but this compound would host diamagnetic Ag(I) and high-spin Co(III). However, at increased pressure ternary fluorides of Ag(II) featuring Cu and Ni could be synthesized, in the pressure windows of 7-14 and 8-15 GPa, respectively. All title compounds would be semiconducting and magnetically ordered.

1. Introduction

Recent experimental and theoretical research on AgF_2 demonstrated that this material mimics very closely the key structural and electronic properties of the well-known lanthanum oxocuprate^[1] (the prototype precursor of high-temperature oxocuprate superconductors). Pristine AgF_2 exhibits strong antiferromagnetic coupling *via* superexchange mechanism in two-dimensional sheets^[2] and substantial mixing of ligand and metal states in the top of the valence band. Because of the striking similarities, not observed in any other known compound, it was suggested that the success of oxocuprates could possibly be repeated by related silver(II) fluorides if chemical doping to AgF_2 could be realized^[1,3,4]. It is therefore highly desirable to examine various possibilities to modify its electronic and magnetic properties *via* doping.

Likewise the oxocuprates, where appropriate doping is required in order to exhibit superconductivity, also fluoroargentates could be doped to achieve this goal. Inserting the surplus holes or electrons is the necessary step towards emergence superconducting transition. However, in contrast to cuprates, the bulk AgF_2 has so far resisted all doping attempts. The hole doping of AgF_2 could be introduced by F^- vacancies, but theoretical studies show that doping to this 001-type system *via* addition or depletion of its F contents does not lead to stable metallic phase^[5]. Partial oxidation of Ag(II) is also difficult, due to immensely strong oxidative character of Ag(III). Therefore, our attention turned to the electron doping, which could be introduced in two ways. The first one could be provided by substitution at anionic sites ($\text{F}^- \rightarrow \text{O}^{2-}$), which will be described elsewhere. Here, we focused on the

second possibility, where doping may be provided by electron injection *via* substitution at cationic site. Therefore, we considered diverse ternary fluoride stoichiometries which may host strongly coupled AgF_2 sheets. Among ternary fluorides $\text{Ag}^{\text{II}}\text{M}_x\text{F}_y$, many transition metal systems have been successfully prepared so far^[3], *i.e.* for $\text{M} = \text{Au(III)}, \text{Au(V)}, \text{Nb(V)}, \text{Ta(V)}, \text{Ti(IV)}, \text{Zr(IV)}, \text{Hf(IV)}, \text{Ru(V)}, \text{Rh(IV)}, \text{Ir(V)}, \text{Pd(IV)}, \text{Pt(IV)}, \text{Pt(V)}, \text{Mn(IV)}$ and Cr(IV) ($\text{AgMn}^{\text{IV}}\text{F}_6$ ^[6] and $\text{AgCr}^{\text{IV}}\text{F}_6$ ^[7] structures not known). The great majority of these compounds contain closed-shell or low-spin M cations. Yet none of these fluorides host $[\text{AgF}_2]$ sheets, as required for doping.

Herein, we theoretically search for systems bearing divalent cations which could possibly host $[\text{AgF}_2]$ sheets using Density Functional Theory (DFT) in combination with evolutionary algorithms for crystal structures' prediction. We examine AgMF_4 systems with transition metals $\text{M} = \text{Cu}, \text{Ni}$ and Co . These late 3d transition metals have been selected due to their relative resistance towards oxidation in the fluoride environment. The redox potentials for the $\text{M}^{3+}/\text{M}^{2+}$ redox pairs decrease in the Cu-Ni-Co sequence. CoF_3 and NiF_3 (actually $\text{Ni}^{\text{II}}\text{Ni}^{\text{IV}}\text{F}_4$ ^[8]) are moderately stable, and they constitute strong fluorinating agents. CuF_3 is rather unstable^[9] (even more than AgF_3 , which structure was determined^[10]), thus minimizing the possibility of the intrinsic redox reaction between Ag(II) and Cu(II) . Aside from variations of the chemical composition, we also study the impact of external pressure on crystal and electronic structure and stability of AgMF_4 systems with respect to the mixture of binary fluorides, AgF_2 and MF_2 ($\text{M}=\text{Co}, \text{Ni}, \text{Cu}$).

2. Methods

This theoretical study is based on periodic electronic-structure calculations carried out with VASP 5.4.4 software using PAW method^[11,12]. We used potentials set recommended by VASP with 520 eV plane-wave energy cut-off. Energy was calculated using collinearly spin-polarized DFT method using GGA functional (PBEsol, *i.e.* solid-revised Perdew, Burke and Ernzerhof correlation-exchange functional^[13]). Geometry optimizations were done with k-spacing of 0.024 \AA^{-1} and conjugate-gradient algorithm relaxation with convergence criteria of 10^{-7} eV (electronic cycle) and 10^{-5} eV (ionic cycle). The tetrahedron method with Blöchl corrections was used to calculate electronic density of states (DOS). On-site electronic correlation was included with Hubbard (U) and exchange repulsion (J) terms using Dudarev's approach^[14,15]. In this approach effective $U_{\text{eff}} = U - J$, is considered, thus we used U_{eff} equal 4 eV (for Ag, Ni), 5 eV (Co) and 8 (Cu). These values were earlier used and validated in respective systems exhibiting +II oxidation state^[2,16-18]. Such choice of U_{eff} is additionally justified by successful confirmation of the experimentally observed pressure induced phase transitions of AgF_2 ^[19], CuF_2 ^[20], NiF_2 ^[21] and CoF_2 ^[16,21] up to 20 GPa (note in **SI**, see also **Table S1** and **Figure S1**). For some systems, geometry optimization was additionally performed using the CPU-consuming HSE06 hybrid functional^[22] with a coarser k-spacing (0.048 \AA^{-1}).

Quest for a lowest-energy structures was performed using particle-swarm evolutionary algorithm, the crystal structure prediction was done utilizing XtalOpt software^[23] in combination with DFT calculations using VASP optimizer. The XtalOpt was utilized *ca.* 60 times in solid state chemistry or physics applications^[24], however most often for binary systems. The cross-check XtalOpt runs were performed for the three title stoichiometries with $Z=2$ or 4 structural units in the unit cell, both at ambient pressure and at 10 GPa, and in each case over 500 distinct structures were generated (with many more duplicates). Manual screening of the Inorganic Crystal Structure Database (ICSD) was also done in search for the appropriate ABC_4 structures, used also as seeds structures in XtalOpt searches. Final optimization of the lowest-energy structures from XtalOpt search and models from ICSD was

performed with the above described DFT+U settings. Using XtalOpt, a four-step optimization of each structure was performed increasing accuracy at each step, with last two using GGA+U approach. VESTA^[25] software was used for visualization of structures. Band structure plots were made using PyProcar library^[26] and AFLOW^[27] program.

3. Results

In our quest for the lowest-energy crystal structure of hypothetical compounds of AgCuF_4 , AgNiF_4 and AgCoF_4 , we have initially tested various substitutions within known crystal structures of AgF_2 , CuF_2 , NiF_2 and CoF_2 from ICSD database. Secondly, XtalOpt evolutionary algorithm was used for the same purpose and for cross-checking the results. Moreover, we have tested various prototypical $\text{M}^{\text{I}}\text{M}^{\text{III}}\text{F}_4$ structures, which allow for electron transfer between metal sites; notably, we presumed that electron-hungry Ag(II) could undergo reduction, with the concomitant 1- or even 2e-oxidation of its neighbouring TM cations. The three scrutinized 3d elements, Co, Ni and Cu, differ in terms of redox properties, electron count, U-induced splitting of upper and lower Hubbard d-bands, and degree of tetragonal distortion of MF_6 octahedra. All above-mentioned cations also have significantly smaller cationic radii than Ag(II) . The hypothetical mixed-cation fluorides are described below one by one, first in terms of structure and electronic properties at ambient pressure. Next, we focus on the pressure-induced stabilization of the proposed ternary phases and also their electronic properties.

Crystal structures and stability of mixed-cation fluorides at ambient pressure

Due to similar chemistry of Ag(II) and Cu(II) as well as similar crystal structures of binary fluorides, our primary candidate for the AgCuF_4 structure was the distorted PdF_2 type structure typical of AgF_2 ^[28]

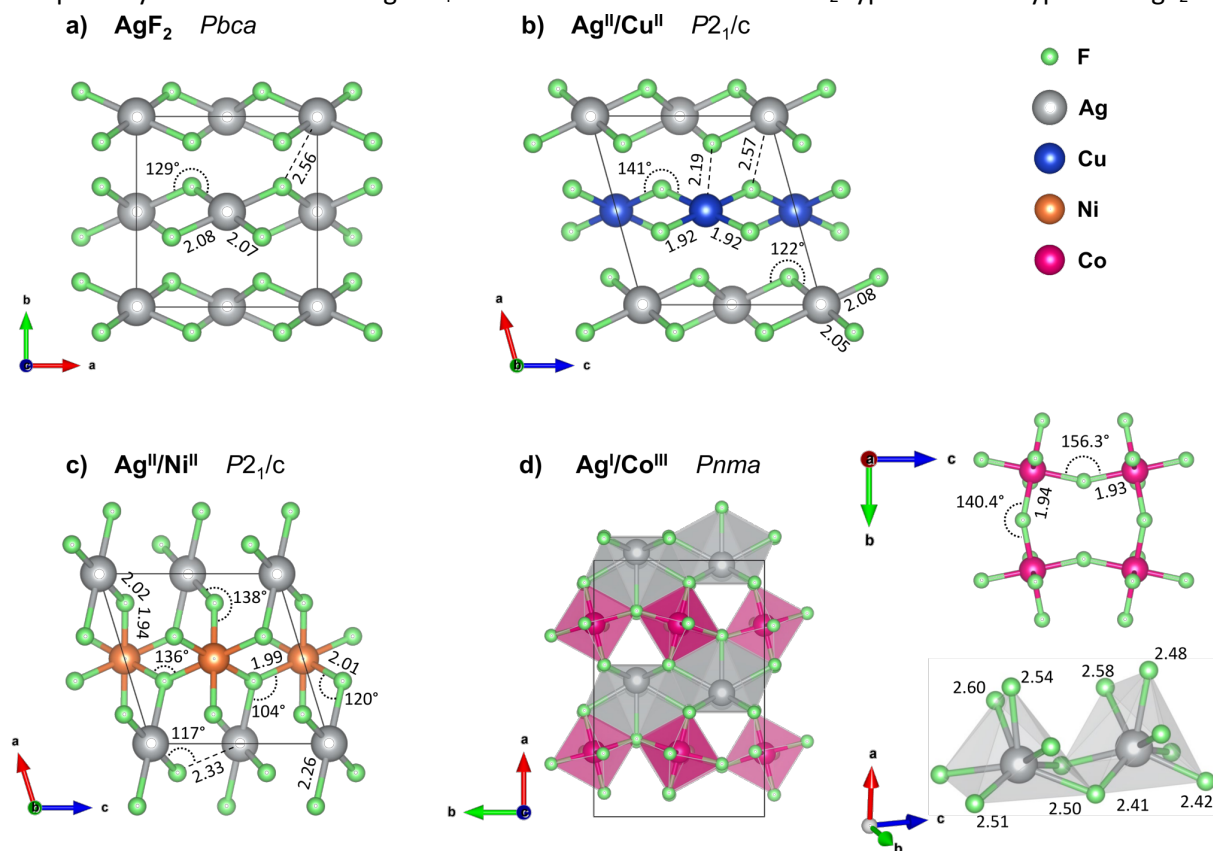
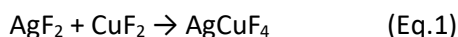


Figure 1. Crystal structures of the lowest-energy predicted AgCoF_4 , AgNiF_4 , AgCuF_4 and parent AgF_2 at ambient pressure (LP structures). The threshold for Ag-F bond drawing is 2.7 Å in $\text{Ag}^{\text{I}}\text{Co}^{\text{III}}\text{F}_4$ structure and 2.3 Å in all other cases. All bond lengths provided in angstroms.

(**Figure 1a**). Three types of substitutions at the metal site were considered, *i.e.* metal alternation in the directions perpendicular to the \vec{a} , \vec{b} or \vec{c} lattice vectors (*cf.* **SI, Figure S2**). Notably, these three diverse polymorphs were also found during XtalOpt search (see **SI, Figure S6**). We found that monoclinic distorted AgF_2 type structure with metal alternation in the a direction is the lowest-energy structure of AgCuF_4 (LP, **Figure 1b**) and this conclusion was confirmed using XtalOpt search; this polymorph preserves layered character of its binary constituents. Substantial tetragonal distortion of both Ag(II) and Cu(II) is predicted in agreement with the strong Jahn-Teller effect which is expected for d^9 species having coordination number (CN) of 6. The tetragonal distorted octahedra usually constitute the $(2 + 2) + 2$ coordination of central atoms, which can be approximated to $(4) + 2$ for the most of cases. In such instance, we calculated the dimensionless Jahn–Teller distortion parameter, which equals the ratio $R = d_{ax}/d_{eq}$. In proposed AgCuF_4 the ratio of axial (2.570 Å) to equatorial (2.065 Å, averaged) bond lengths equals 1.24 for the Ag(II) site and 1.14 for the Cu(II) one (with axial bond lengths of 2.188 Å and equatorial ones of 1.919 Å). For comparison, the R ratio equals to 1.23 and 1.18, for AgF_2 and CuF_2 , respectively. The AgCuF_4 forms antiferromagnetic $[\text{AgF}_{4/2}]$ and $[\text{CuF}_{4/2}]$ separate layers inside crystal lattice (consequently, this polymorph is labelled as SL). The geometry within the puckered layers is reminiscent of those found in binary fluorides; the $[\text{AgF}_2]$ layers are more buckled than in pure AgF_2 (the Ag-F-Ag angle is 122.0° vs. 129.1° in bulk AgF_2), while $[\text{CuF}_2]$ layers are flattened (the corresponding angle is 140.8° vs. 131.8° in bulk CuF_2). This feature obviously stems from difference of the ionic radii between Ag(II) and Cu(II) . In order to form a segregated layer structure without much strain the $[\text{AgF}_2]$ sheets must buckle and the $[\text{CuF}_2]$ sheets must simultaneously flatten; this accommodation is associated by bending of the crystallographic beta angle from 90° (for bulk AgF_2) to 105.5° . Interestingly, several higher energy crystal structures either contain Ag-F-Cu bridges and they preserve layered character (as it is the case for the polymorphs with metal substitutions $\perp \vec{a}$ and $\perp \vec{c}$), or they exhibit genuine 3D connectivity (**SI, Figure S2**). Importantly, the most stable SL polymorph is computed to be +6.7 kJ/mol uphill in energy with respect to substrates:

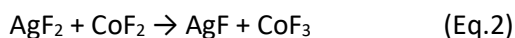


Thus, it should not dissociate to the binaries at $p \rightarrow 0$ GPa, $T \rightarrow 0$ K conditions. If, however, it could be achieved in experiment, it would be metastable with respect to phase separation.

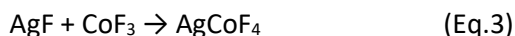
Predictions of the crystal structure of AgNiF_4 – in contrast to those featuring Cu(II) – were influenced by the fact that Ni(II) reveals a known tendency to be oxidized to Ni(III) or even Ni(IV) (though higher fluorides of nickel tend to release F_2).^[29] However, during our quest only very few such structures with intervalence charge transfer were found, having considerably higher enthalpy (*i.e.* at least +0.620 eV, *cf.* **SI, Figure S6**). Similarly, as in the case of Cu(II) , the final lowest-energy structure can be derived from parent AgF_2 type structure, however it is not layered. The electronic ground state of this ternary fluoride is antiferromagnetic. In contrast to the parent NiF_2 (tetragonal rutile structure) and AgF_2 the lowest-energy AgNiF_4 has monoclinic structure with beta angle 107.1° . In the mixed cation fluoride one can distinguish the Ag(II) site forming AgF_6 octahedron with shorter axial bond (2.025 Å) and two longer Ag-F bonds (2.260 and 2.332 Å, **Figure 1c**), which is octahedrally compressed with R ratio equal *ca.* 0.88. The tetragonal compression of octahedra is well known from the fluorine chemistry of Ag(II) .^[30] On the other hand, the NiF_6 octahedra are nearly undistorted with axial bonds lengths of 1.941 Å and equatorial ones of 1.995 and 2.008 Å. In the LP structure Ag(II) cations act as connectors between $[\text{NiF}_{4/2}\text{F}_{2/1}]^{2-}$ layers present within the *bc* plane. However, the Ag-F bonds involved in formation of the Ag-F-Ni bridges are shorter than the Ag-F bonds forming Ag-F-Ag' bridges (**Table 1**). This LP structure was labelled 3D due to its spatial connectivity and its lowest-energy among all structures found at 0

GPa, but it still has energy +8.6 kJ/mol with respect to the binary substrates $\text{AgF}_2 + \text{NiF}_2$. In conclusion, if synthesized, AgNiF_4 could be metastable at ambient pressure.

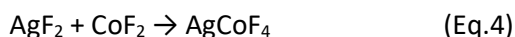
In the case of AgCoF_4 , the difference between standard reduction potentials for the $\text{Co}^{3+/2+}$ and $\text{Ag}^{2+/1+}$ redox pairs is considerable (1.82 V vs. 1.98 V^[31], respectively), so a facile reaction:



could be expected. Calculations show that this reaction would not be favoured though, on both DFT+U level of theory (+25.8 kJ/mol) or hybrid density functional HSE06 (+12.2 kJ/mol, see HSE06 results for all the binary and ternary compounds in **SI, Table S2**). Nevertheless, it appears that the lowest-energy obtained mixed-cation structure corresponds in fact to the $\text{Ag}^{\text{I}}\text{Co}^{\text{III}}\text{F}_4$ formulation; this is because enthalpy for the Lewis acid-Lewis base reaction:



is negative, some -30.1 kJ/mol at DFT level (-37.1 kJ/mol with hybrid functional). The spontaneous redox reaction (which manifests itself by disappearance of the spin on Ag site, and modification of magnetic moment on the Co site) is seen even for the models derived from parent AgF_2 type structure. The lowest-energy polymorph found was $\text{KFeF}_4\text{-LT}^{\text{[32]}}$ type structure ($Z=8$, **Figure 1d**). DFT+U calculations yield energy of this structure to be -4.2 kJ/mol (-24.8 at HSE06 level) with respect to the binary divalent metal fluorides:



Further structure quests with XtalOpt resulted in many similar, layered $\text{Ag}^{\text{I}}\text{Co}^{\text{III}}\text{F}_4$ structures, including $\text{KFeF}_4\text{-HT}$ polymorph ($Z=4$, for other see **SI, Figure S6**). The $\text{KFeF}_4\text{-LT}$ type crystal structure comprises the puckered antiferromagnetic anionic sheets of $[\text{CoF}_{4/2}\text{F}_{2/1}]^-$ stoichiometry which feature high-spin $\text{Co}(\text{III})$ cations, and diamagnetic $\text{Ag}(\text{I})$ acting as counterion. While in parent CoF_3 the octahedra are almost perfectly symmetric (with all bond lengths of 1.886 Å, the F-Co-F angles are distorted $\pm 1.5^\circ$ from 90°), in AgCoF_4 the CoF_6 octahedra are markedly compressed with axial bond length 1.824 Å and two equatorial ones of $1.93\text{--}1.95$ Å (ratio of *ca.* 0.94). The axial Co-F bonds are oriented towards $\text{Ag}(\text{I})$ layer, while equatorial bonds form a layer parallel to *bc* plane with angles 140.4° and 156.3° on Co-F-Co bridges; for comparison, the corresponding angles found in binary CoF_3 are 149.3° . Considering coordination sphere of $\text{Ag}(\text{I})$, pristine AgF crystalizes in rock-salt structure with perfect octahedra having 2.426 Å Ag-F bond lengths. In the case of AgCoF_4 however, two types of $\text{Ag}(\text{I})$ can be distinguished, but each $\text{Ag}(\text{I})$ has CN=7 within 2.65 Å radius which form bicapped tetragonal pyramid. One $\text{Ag}(\text{I})$ site exhibits $2.41\text{--}2.42$ Å bond lengths to fluoride anions within tetragonal base, 2.482 Å in the apex and 2.576 Å for the two capping fluorides; the other $\text{Ag}(\text{I})$ site features $2.50\text{--}2.51$ Å, 2.537 Å and 2.602 Å bond lengths, respectively. Two more distant fluoride ions are found at 2.767 Å.

Crystal structures of high-pressure polymorphs at 10 GPa

Pressure may affect to a great extent both the crystal structures and stability of chemical compounds.^[33] Here we have examined the impact of a rather moderate pressure of up to 20 GPa on formation of the title AgMF_4 compounds.

Pressure increase from 0 to 10 GPa in AgCuF_4 system turns out to promote the formation of the HP1 (3D) structure exhibiting spatial connectivity (**Figure 2b**) rather than the layers structure obtained at 0 GPa **Figure 1b**). The HP1 (3D) polytype is based on AgF_2 type structure with the shortest Ag-F bonds involved in the formation of strong Ag-F-Cu bridges (**Figure 2b**). This polymorph has already been identified as a low-volume polymorph at ambient pressure in our XtalOpt quest. It is enthalpically preferred over LP (SL) polymorph starting from about 6 GPa (**Figure 3a**). The HP1 form of AgCuF_4 has ferrimagnetic character with small uncompensated spin (*ca.* $0.02 \mu_B$) due to opposite spin on $\text{Ag}(\text{II})$ and $\text{Cu}(\text{II})$ cations with slightly differing magnetic moments on each type of TM cation. Like in the low-

pressure polymorph, here the Cu and Ag octahedra are orthorhombically distorted and tetragonally elongated, respectively. In the case of Ag-F bonds, the axial contacts are equal to 2.382 Å and the equatorial ones are 2.030 Å and 2.099 Å (with average ratio, R , of 1.15) while Cu-F bonds have three different lengths of 2.148 Å, 1.848 Å and 1.905 Å, respectively. As mentioned, dominant structural motifs in this crystal structure are the Ag-F-Cu bridges along directions [101] and [110] forming infinite antiferromagnetic chains. Chains along [110] feature 2.030 Å Ag-F and 1.848 Å Cu-F bond lengths with 133.6° angle while those along [101] are built from 2.099 Å Ag-F and 1.905 Å Cu-F bonds at 120.4° angle.

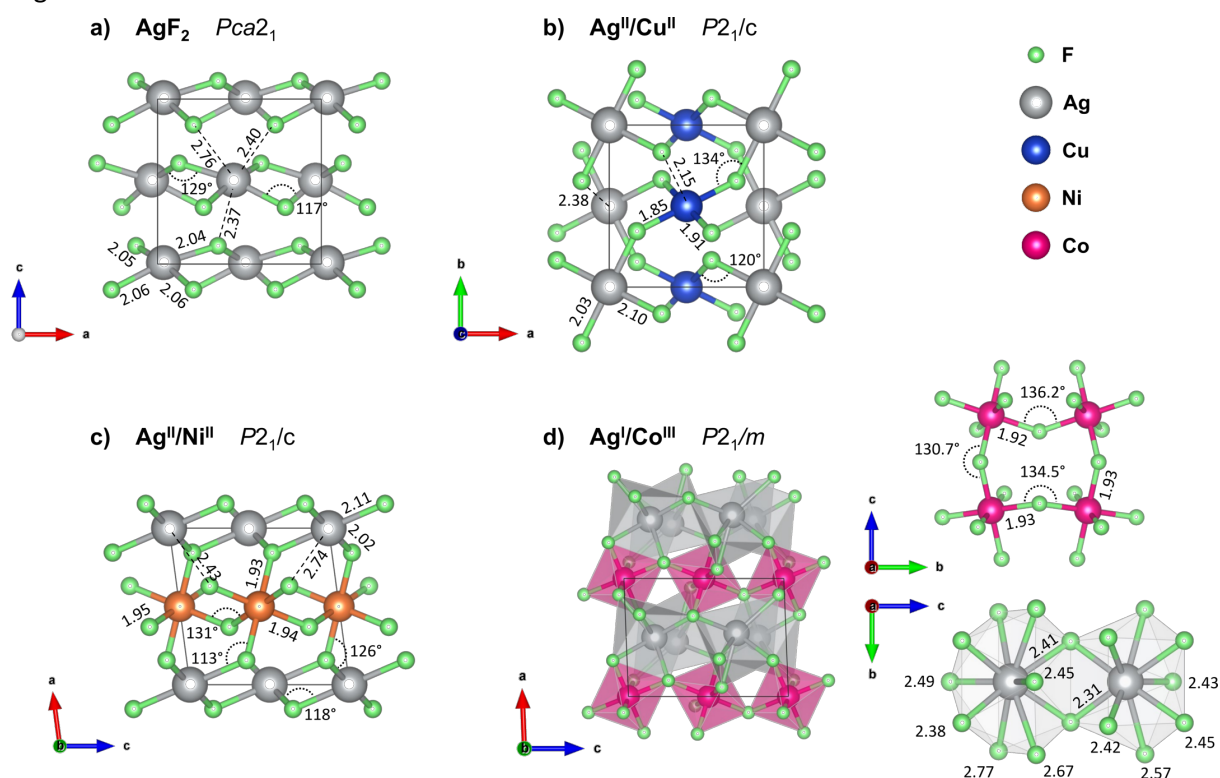


Figure 2. Crystal structures of the lowest-enthalpy predicted AgCoF_4 , AgNiF_4 , AgCuF_4 and parent AgF_2 at 10 GPa.

Also in AgNiF_4 system we predict change in relative stability of diverse polymorphs. In contrast to AgCuF_4 , here the layered structure (HP1, **Figure 2c**) gains stability under pressure with respect to the 3D polymorph. The HP1 (SL) polymorph can be viewed as consisting of separate antiferromagnetic layers of AgF_2 and NiF_2 parallel to bc plane. In this structure, both Ag-F bonds within AgF_2 layer are considerably shorter (2.021 Å and 2.112 Å) than the axial Ag-F bond (2.433 Å, corresponding to an average R factor of 1.18) which connects AgF_2 and NiF_2 layers. Also, the Ag-F-Ag angle within antiferromagnetic AgF_2 layer is rather far from straight (117.7°), and comparable with those computed for the HP1 polymorph of AgF_2 of 116.9° and 129.1° (**Figure 2a**). Simultaneously, the shortest Ni-F bonds at 1.927 Å connect Ni(II) with AgF_2 layer indicating a possibility of a strong magnetic interaction between both cations; the Ag-F-Ni angle equals 125.8°. Indeed, these magnetic centres form antiferromagnetic chains along [1 -1 0] direction. The HP1 (SL) structure of AgNiF_4 was found to be preferred over the LP polytype starting from 3 GPa and has negative enthalpy as compared to the binary fluorides from the pressure of 7 GPa (**Figure 3b**).

High pressure polymorph of AgCoF_4 found at 10 GPa preserves the layered-type structure found for the LP polymorph. The distorted monoclinic KMnF_4 -related structure found using XtalOpt (HP1, **Figure 2d**) is preferred over the KFeF_4 -LT type structure starting from the pressure of ~2 GPa

(Figure 3c). This polymorph resembles LP polymorph in having antiferromagnetic puckered sheets of $[\text{CoF}_{4/2}\text{F}_{2/1}]^-$ stoichiometry with high-spin Co(III) cations and diamagnetic Ag(I) in between. Antiferromagnetic sheets are built from CoF_6 octahedra exhibiting tetragonal compression *i.e.* with short axial (1.78 Å) and longer equatorial bond lengths (1.92–1.93 Å) with *R* factor of about 0.92 at 10 GPa. These equatorial bonds form a layer parallel to *bc* plane with Co-F-Co angles equal to 130.7°, 134.5° and 136.2°. The second constituent of $\text{Ag}^{\text{I}}\text{Co}^{\text{III}}\text{F}_4$ at 10 GPa, the Ag(I) cation, is found in two distinct crystallographic sites which differ in their coordination number. Here, CN is either 9 or 10, with bond lengths varying from 2.31 up to 2.77 Å (**Figure 2d**). At the same pressure, parent AgF transforms into CsCl type structure with cubic coordination sphere (8 ligands) and Ag-F bond length of 2.47 Å. Volume decrease of $\text{Ag}^{\text{I}}\text{Co}^{\text{III}}\text{F}_4$ with respect to binary fluorides is mainly due to enhancement of $[\text{CoF}_{4/2}\text{F}_{2/1}]^-$ buckling and increase of Ag(I) coordination number.

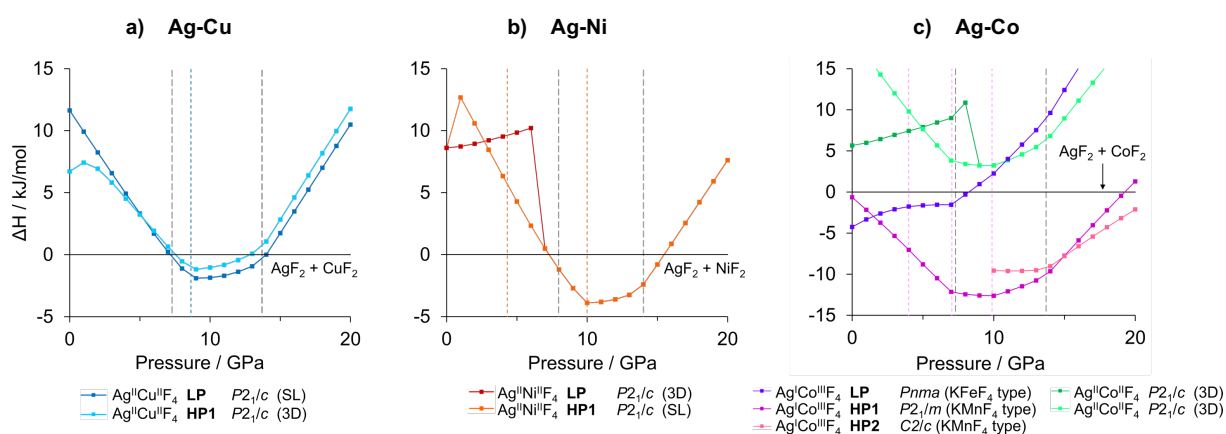


Figure 3. Calculated relative enthalpy of ternary silver fluorides AgMF_4 ($M = \text{Ni}, \text{Co}, \text{Cu}$) with respect to lowest-enthalpy polymorphic forms of substrates at each given pressure point. All the lowest enthalpy Ag(II)-M(II) fluorides comprise M-half-substituted AgF_2 type structures. Vertical dashed lines indicate phase transitions calculated for the MF_2 substrates. SL stands for the cation separated-layers polymorphs of $\text{Ag}^{\text{II}}\text{M}^{\text{II}}\text{F}_4$ while 3D denotes the spatially bonded.

Evolution of stability with external pressure

The pressure evolution of enthalpy for AgMF_4 systems ($M = \text{Cu}, \text{Ni}$ and Co) with respect to the sum of those for the binary substrates in their most stable polymorphs is presented in **Figure 3**. The phase-transition sequences in the considered stoichiometries were calculated with GGA+U assuming hydrostatic conditions.

AgCuF_4 HP1 polymorph (3D) is enthalpically favoured with respect to the substrates in the pressure range about 7-14 GPa with the minimum relative enthalpy at ca. 9 GPa (by -1.9 kJ/mol, **Figure 3a**). Similar pressure-induced stability is predicted for AgNiF_4 system HP1, with the separate layers (SL) structure gaining its stability under high-pressure (**Figure 3b**). The range of stability of the AgNiF_4 system is predicted to be about 7-15 GPa, with the maximum stabilization of -3.9 kJ/mol at 10 GPa relative to binary substrates. Due to small structural differences between both proposed structures of AgNiF_4 it may be expected, that if HP1 structure was synthesized under high-pressure it would decompress to their LP forms without large internal strain. In fact, during standard geometry optimization a smooth transition between both HP1 (SL) and LP (3D) polymorphs occurred (*i.e.* optimization of HP polymorph at 0 GPa gave LP structure and also optimization of LP polymorph at 10 GPa led to HP structure).

As mentioned before, the $\text{Ag}^{\text{I}}\text{Co}^{\text{III}}\text{F}_4$ system is stable with respect to divalent binary fluorides even at ambient pressure. Apparently, it turns out that $\text{Ag}^{\text{I}}\text{Co}^{\text{III}}\text{F}_4$ stability would increase almost threefold with respect to substrates at 10 GPa, up to -12.6 kJ/mol, due to phase transition into monoclinic distorted KMnF_4 type polymorph HP1. Another, yet also monoclinic distorted KMnF_4 type polymorph HP2 ($C2/c$) with $\text{CN}=10$ for all $\text{Ag}(\text{I})$, was found to predominate the phase diagram of $\text{Ag}^{\text{I}}\text{Co}^{\text{III}}\text{F}_4$ system from 15 GPa for up to 22 GPa (**Figure 3c**, with linear extrapolation used to estimate transition pressure above 20 GPa). Interestingly, hypothetical $\text{Ag}^{\text{I}}\text{Co}^{\text{II}}\text{F}_4$ adopting AgF_2 type structures, *i.e.* similar to those of AgCuF_4 and AgNiF_4 , would not be stabilized under high pressure (**Figure 3c** green curves).

Additional insight into pressure-induced effects on enthalpy of formation come from pV term analysis (**SI, Figure S3**). Both for relatively low pressure (< 3 GPa) and high pressure range (> 9 GPa) the pV factor works against formation of ternary fluoride phases. Simultaneously, ternary fluoride phases benefit from the pV term with respect to the substrates in the range 3–9 GPa; at higher pressures binary substrates experience volume-reducing phase transitions which reduces the said advantage. The crucial is the 2nd phase transition of AgF_2 at ~ 14 GPa, which reduces the pV term of substrates and gradually destabilizes thermodynamically all proposed ternary fluorides at pressures approaching 20

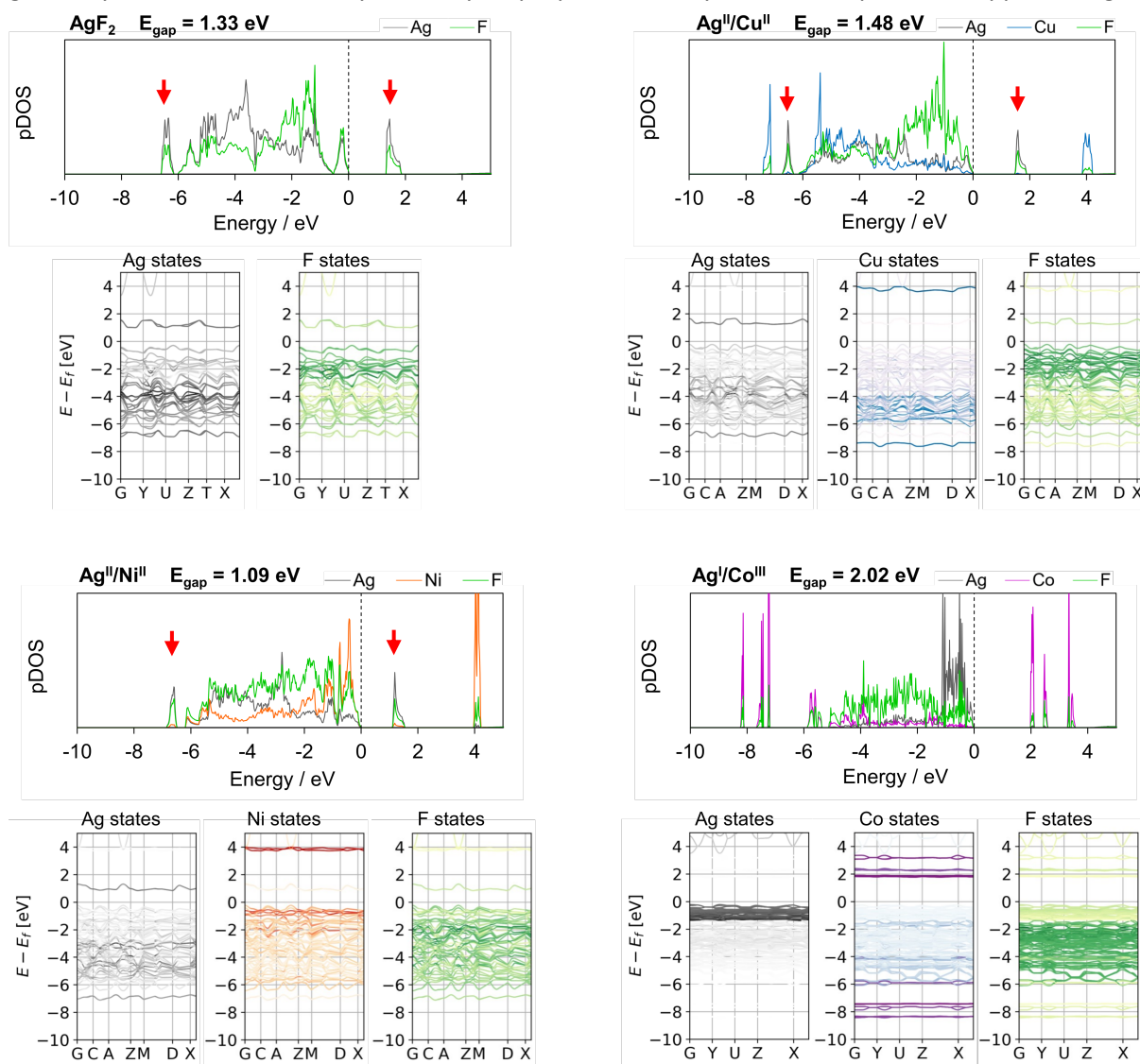


Figure 4. Top: Orbital projected electronic density of states (pDOS) of the parent AgF_2 and proposed AgCuF_4 , AgNiF_4 , AgCoF_4 compounds. Red arrows indicate lower and upper Hubbard (LHB and UHB) bands of Ag. **Bottom:** Band structure plots inside first Brillouin zone of the unit cells, where color intensity indicates respective element contribution (0-100%).

GPa. These factors result in re-entrant instability of ternary phases above certain characteristic pressure in each case.

Electronic properties

Electronic density of states (DOS) and band structures for the title compounds and AgF₂ reference at ambient pressure are shown in **Figure 4**. Results of electronic structure calculations for the parent AgF₂ agree with previously published DFT+U results: it shows a narrow band gap (1.33 eV) with strongly

Table 1. Summary of the lowest-enthalpy structures predicted for AgCoF₄, AgNiF₄, AgCuF₄ and parent AgF₂ at ambient pressure, 10 GPa and 20 GPa. Calculated energies or enthalpies of formation, electronic band gaps and lengths of the three shortest Ag-F bonds are provided. The bond lengths describe AgF₆ octahedra distortion except in the case of AgCoF₄ structures. For the relative volume relation, see **Figure S3**.

mixture of Ag 4d and F 2p orbitals around the Fermi level^[1,18]. Overall, AgF₂ is a charge-transfer (CT) insulator according to Zaanen-Sawatzky-Allen classification scheme.^[34]

Structure at 0 GPa			ΔE_f / kJ/mol	E_{gap} / eV	bond length / Å		
System	Structure type	Symmetry			Ag-F ₁	Ag-F ₂	Ag-F ₃
AgF ₂	LP AgF ₂	<i>Pbca</i>	-	1.334	2.072	2.075	2.560
AgCuF ₄	LP AgF ₂ type (SL)	<i>P2₁/c</i>	6.7	1.484	2.049	2.071	2.598
AgNiF ₄	LP AgF ₂ type (3D)	<i>P2₁/c</i>	8.6	0.902	2.025	2.260	2.332
AgCoF ₄	LP KFeF ₄ type	<i>Pnma</i>	-4.2	2.020	2.411	2.482	2.504

Structure at 10 GPa			ΔH_f / kJ/mol	E_{gap} / eV	bond length / Å		
System	Structure type	Symmetry			Ag-F ₁	Ag-F ₂	Ag-F ₃
AgF ₂	HP1 AgF ₂	<i>Pca2₁</i>	-	1.311	2.056	2.061	2.369
AgCuF ₄	HP1 AgF ₂ type (3D)	<i>P2₁/c</i>	-1.9	1.512	2.061	2.105	2.604
AgNiF ₄	HP1 AgF ₂ type (SL)	<i>P2₁/c</i>	-3.9	0.618	2.021	2.112	2.433
AgCoF ₄	HP1 KMnF ₄ type dist.	<i>P2₁/m</i>	-12.6	1.786	2.313	2.379	2.411

Structure at 20 GPa			ΔH_f / kJ/mol	E_{gap} / eV	bond length / Å		
System	Structure type	Symmetry			Ag-F ₁	Ag-F ₂	Ag-F ₃
AgF ₂	HP2 AgF ₂	<i>Pbcn</i>	-	1.288	2.048	2.063	2.643
AgCuF ₄	HP1 AgF ₂ type (3D)	<i>P2₁/c</i>	10.5	1.493	2.002	2.075	2.303
AgNiF ₄	HP1 AgF ₂ type (SL)	<i>P2₁/c</i>	7.6	0.629	1.992	2.080	2.351
AgCoF ₄	HP2 KMnF ₄ type dist.	<i>C2/c</i>	-2.1	2.009	2.338	2.376	2.401

Analysis of AgCuF₄ electronic DOS at 0 GPa shows that Cu states are not admixing significantly to the states around Fermi level but they form a pair of Hubbard bands which are well-split from those characteristic of Ag. AgCuF₄ has a slightly broader band gap than parent AgF₂ (1.48 eV vs. 1.33 eV), while preserving its insulator character associated with a ligand to metal charge transfer (LMCT). Increasing the pressure up to 10 GPa and transition to the HP polymorph keeps the AgCuF₄ band gap nearly constant (**Figure S4**, at about 1.51 eV), as typical for the compounds of d⁹ cations.

Calculations of electronic DOS for AgNiF₄ yield noticeably narrower band gap than in parent AgF₂ (1.09 eV). Interestingly, in this case valence states of all three constituting elements mix firmly within the valence band, but the Ag(II) contribution is now smaller than for pristine AgF₂. The valence band region is composed predominantly from F and Ni(II) states, while the conduction band preserves the character of Ag UHB band level. Under elevated pressure of 10 GPa the band gap of AgNiF₄ narrows down to 0.62 eV, which is less than half of parent AgF₂ at the same pressure (*cf.* HP evolution of electronic band gaps of ternary fluorides and AgF₂ in **SI, Figure S7**). These features suggest the inter-valence charge transfer (IVCT) character of AgNiF₄ and a certain propensity towards redox process yielding higher oxidation states of Ni, with a concomitant reduction of Ag(II) to Ag(I).

In the case of AgCoF_4 the band gap at ambient pressure is 2.02 eV thus much larger than those of pristine binary fluorides (**Figure 4**). The top of valence band mainly consists of filled d states of Ag(I) while the bottom of conduction band corresponds to the UHB of Co(III). Due to intrinsic redox reaction character, the band gap of $\text{Ag}^{\text{I}}\text{Co}^{\text{III}}\text{F}_4$ has an intervalence charge transfer (IVCT) character, with Ag(I) serving as an electron donor, and Co(III) as an acceptor. At 10 GPa band gap of $\text{Ag}^{\text{I}}\text{Co}^{\text{III}}\text{F}_4$ decreases noticeably down to 1.79 eV, but it is still about 0.5 eV larger than the corresponding gap for AgF_2 HP1 type.

Clearly, electronic structure of AgMF_4 compounds in the series $\text{M}=\text{Cu, Ni, Co}$, changes quite predictably with the redox properties of M(II) cations. For $\text{M}=\text{Cu}$, with Cu(III) oxidation state experimentally accessible with the greatest difficulty, AgCuF_4 preserves Ag(II) and Cu(II) oxidation states and a LMCT insulator character. For $\text{M}=\text{Ni}$, where Ni(III) oxidation state forms easier, electronic DOS of AgNiF_4 reveals a moderate ease of IVCT between Ni(II) donor and Ag(II) acceptor, with the corresponding valence and conduction bands separated by a mere ~ 1.1 eV. Finally, for $\text{M}=\text{Co}$, where Co(III) is most accessible, genuine redox reaction is seen which leads to “inverse” IVCT character – now Ag(I) serves as an electron donor, while Co(III) as an acceptor.

4. Conclusions

The silver(II) fluoride system is theoretically predicted to resist forming ternary fluorides with Cu, and Ni fluorides at ambient pressure conditions. The energy of formation of $\text{Ag}^{\text{II}}\text{Cu}^{\text{II}}\text{F}_4$ and $\text{Ag}^{\text{II}}\text{Ni}^{\text{II}}\text{F}_4$ are positive (+6.7 kJ/mol and +8.6 kJ/mol respectively), thus they could be only metastable if prepared. At ambient pressure, $\text{Ag}^{\text{II}}\text{Cu}^{\text{II}}\text{F}_4$ shows layered structure with buckled $[\text{AgF}_2]$ layers, similar as in parent AgF_2 . Also, the lowest-energy structure of $\text{Ag}^{\text{II}}\text{Ni}^{\text{II}}\text{F}_4$ stems from AgF_2 structure, but it forms 3D polymorph showing strong Ag-Ni bonds where Ag(II) acts like connector between $[\text{NiF}_{4/2}\text{F}_{2/1}]^{2-}$ layers. Both $\text{Ag}^{\text{II}}\text{Cu}^{\text{II}}\text{F}_4$ and $\text{Ag}^{\text{II}}\text{Ni}^{\text{II}}\text{F}_4$ are predicted to be semiconductors with predominant LMCT and IVCT character, respectively. AgCuF_4 system has a larger calculated band gap than that for pristine AgF_2 at ambient pressure (for AgF_2 1.33 eV and 1.48 eV for AgCuF_4 LP), while AgNiF_4 system features a significantly narrower band gap (1.09 eV for AgNiF_4 LP).

The cobalt-silver fluoride system is quite different from the other two due to intrinsic redox reaction resulting in spontaneous formation of $\text{Ag}^{\text{I}}\text{Co}^{\text{III}}\text{F}_4$ in the KFeF_4 type. The ambient-pressure AgCoF_4 is computed to be a *ca.* 2.02 eV band gap semiconductor with IVCT character of the gap, featuring antiferromagnetic sheets of $[\text{CoF}_{4/2}\text{F}_{2/1}]^-$ stoichiometry, stable by -4.2 kJ/mol with respect to binary fluorides.

Application of hydrostatic pressure in our calculations shows that there is a pressure range where formation of ternary silver fluorides $\text{Ag}^{\text{II}}\text{M}^{\text{II}}\text{F}_4$ is favoured. The range of stability is about 7-15 GPa for AgCuF_4 , 8-15 GPa for AgNiF_4 , and 0-22 GPa for AgCoF_4 . Nickel system is noteworthy, because at 10 GPa it should form the separate layers polymorph with quite narrow band gap (0.62 eV, less than half of that for AgF_2) and simultaneously slightly negative enthalpy of formation -3.9 (kJ/mol) with respect to substrates. Finally, for AgCoF_4 the ambient pressure KFeF_4 -LT type is calculated to yield to distorted monoclinic KMnF_4 type structure in the pressure range of 1.5-19 GPa.

Acknowledgments: This work was supported by Polish National Science Center (NCN) within Beethoven project (2016/23/G/ST5/04320). The research was carried out using supercomputers of Interdisciplinary Centre for Mathematical and Computational Modelling (ICM), University of Warsaw, under grant number GA76-19. Dr Derzsi acknowledges the ERDF, R&I Operational Program

(ITMS2014+: 313011W085), Scientific Grant Agency of the Slovak Republic grant (VG 1/0223/19) and the Slovak Research and Development Agency grant (APVV-18-0168).

References

- [1] J. Gawraczyński, D. Kurzydłowski, R. A. Ewings, S. Bandaru, W. Gadomski, Z. Mazej, G. Ruani, I. Bergenti, T. Jaroń, A. Ozarowski, S. Hill, P. J. Leszczyński, K. Tokár, M. Derzsi, P. Barone, K. Wohlfeld, J. Lorenzana, W. Grochala, *PNAS* **2019**, *116*, 1495–1500.
- [2] D. Kurzydłowski, M. Derzsi, P. Barone, A. Grzelak, V. Struzhkin, J. Lorenzana, W. Grochala, *Chemical Communications* **2018**, *54*, 10252–10255.
- [3] W. Grochala, R. Hoffmann, *Angewandte Chemie International Edition* **2001**, *40*, 2742–2781.
- [4] W. Grochala, Z. Mazej, *Philosophical Transactions of the Royal Society A: Mathematical, Physical and Engineering Sciences* **2015**, *373*, 20140179.
- [5] A. Grzelak, *manuscript in preparation* **2020**.
- [6] R. Hoppe, G. Siebert, *Zeitschrift für anorganische und allgemeine Chemie* **1970**, *376*, 261–267.
- [7] G. Stebert, R. Hoppe, *Naturwissenschaften* **1971**, *58*, 95–96.
- [8] C. Shen, L. C. Chacón, N. Rosov, S. H. Elder, J. C. Allman, N. Bartlett, *Comptes Rendus de l'Académie des Sciences - Series IIC - Chemistry* **1999**, *2*, 557–563.
- [9] N. Bartlett, G. Lucier, C. Shen, W. J. Casteel, L. Chacon, J. Munzenberg, B. Žemva, *J. Fluor. Chem.* **1995**, *71*, 163–164.
- [10] B. Zemva, K. Lutar, A. Jesih, W. J. Casteel, A. P. Wilkinson, D. E. Cox, R. B. Von Dreele, H. Borrmann, N. Bartlett, *J. Am. Chem. Soc.* **1991**, *113*, 4192–4198.
- [11] G. Kresse, J. Furthmüller, *Phys. Rev. B* **1996**, *54*, 11169–11186.
- [12] G. Kresse, D. Joubert, *Phys. Rev. B* **1999**, *59*, 1758–1775.
- [13] J. P. Perdew, A. Ruzsinszky, G. I. Csonka, O. A. Vydrov, G. E. Scuseria, L. A. Constantin, X. Zhou, K. Burke, *Phys. Rev. Lett.* **2008**, *100*, 136406.
- [14] A. I. Liechtenstein, V. I. Anisimov, J. Zaanen, *Phys. Rev. B* **1995**, *52*, R5467–R5470.
- [15] S. L. Dudarev, G. A. Botton, S. Y. Savrasov, C. J. Humphreys, A. P. Sutton, *Phys. Rev. B* **1998**, *57*, 1505–1509.
- [16] J. A. Barreda-Argüeso, S. López-Moreno, M. N. Sanz-Ortiz, F. Aguado, R. Valiente, J. González, F. Rodríguez, A. H. Romero, A. Muñoz, L. Nataf, F. Baudelet, *Phys. Rev. B* **2013**, *88*, 214108.
- [17] M. Cococcioni, S. de Gironcoli, *Phys. Rev. B* **2005**, *71*, 035105.
- [18] C. Miller, A. S. Botana, *Phys. Rev. B* **2020**, *101*, 195116.
- [19] A. Grzelak, J. Gawraczyński, T. Jaroń, D. Kurzydłowski, A. Budzianowski, Z. Mazej, P. J. Leszczyński, V. B. Prakapenka, M. Derzsi, V. V. Struzhkin, W. Grochala, *Inorg. Chem.* **2017**, *56*, 14651–14661.
- [20] D. Kurzydłowski, *Crystals* **2018**, *8*, 140.
- [21] L. C. Ming, M. H. Manghnani, T. Matsui, J. C. Jamieson, *Phys. Earth Planet. Inter.* **1980**, *23*, 276–285.
- [22] A. V. Krukau, O. A. Vydrov, A. F. Izmaylov, G. E. Scuseria, *J. Chem. Phys.* **2006**, *125*, 224106.
- [23] D. C. Lonie, E. Zurek, *Computer Physics Communications* **2011**, *182*, 372–387.
- [24] "XtalOpt - Publications," can be found under <http://xtalopt.github.io/pub.html>, **2020**.
- [25] K. Momma, F. Izumi, *J Appl Cryst* **2011**, *44*, 1272–1276.
- [26] U. Herath, P. Tavadze, X. He, E. Bousquet, S. Singh, F. Muñoz, A. H. Romero, *Computer Physics Communications* **2020**, *251*, 107080.
- [27] W. Setyawan, S. Curtarolo, *Computational Materials Science* **2010**, *49*, 299–312.
- [28] P. Fischer, G. Roullet, D. Schwarzenbach, *Journal of Physics and Chemistry of Solids* **1971**, *32*, 1641–1647.
- [29] B. Zemva, K. Lutar, L. Chacon, M. Fele-Beuermann, J. Allman, C. Shen, N. Bartlett, *J. Am. Chem. Soc.* **1995**, *117*, 10025–10034.
- [30] W. Grochala, *physica status solidi (b)* **2006**, *243*, R81–R83.
- [31] A. J. Bard, R. Parsons, J. Jordan, International Union of Pure and Applied Chemistry, *Standard Potentials in Aqueous Solution*, M. Dekker, New York, **1985**.
- [32] J. Lapasset, P. Sciau, J. Moret, N. Gros, *Acta Cryst B* **1986**, *42*, 258–262.
- [33] W. Grochala, R. Hoffmann, J. Feng, N. W. Ashcroft, *Angewandte Chemie International Edition* **2007**, *46*, 3620–3642.
- [34] J. Zaanen, G. A. Sawatzky, J. W. Allen, *Phys. Rev. Lett.* **1985**, *55*, 418–421.
- [35] S. Hull, P. Berastegui, *J. Phys.: Condens. Matter* **1998**, *10*, 7945–7955.

Supporting information

Theoretical study of ternary silver fluorides AgMF_4 ($M = \text{Co}, \text{Ni}, \text{Cu}$) formation at pressures up to 20 GPa

M.A. Domański^{1*}, M. Derzsi^{1,2} and W. Grochala^{1*}

Contents

- S1. Estimated phase-transition pressures for the substrates
- S2. Supplementary Figures
- S3. Supplementary Tables
- S4. Crystal structures in POSCAR format

S1. Estimated phase-transition pressures for the substrates

The calculations were performed for the pressures up to 20 GPa, thus we considered the known phase transitions (PTs) for AgF_2 ^[19] (sequence $Pbca \rightarrow Pca2_1$ (~8 GPa) $\rightarrow Pbcn$ (~14 GPa)), AgF ^[35] (NaCl-type \rightarrow CsCl-type (1-3 GPa)), CoF_2 ^[16,21] (rutile $\rightarrow Pnmm$ (~4 GPa) $\rightarrow Pbca/Pa\bar{3}$ (~8 GPa) $\rightarrow I4/mmm$ (~12 GPa)), NiF_2 ^[21] (rutile $\rightarrow Pnmm$ (~4 GPa) $\rightarrow I4/mmm$ (~10 GPa)) and CuF_2 ^[20] ($P2_1/c \rightarrow Pbca$ (~9 GPa)).

Our results are presented on the **Figure S1** and in the **Table S1**. All of the abovementioned PTs were confirmed using chosen theoretical approach, resulting in PT pressure differences smaller than 1.0 GPa (the only exception is nearly 2 GPa shift for 3rd PT of CoF_2). We indicate also that so called in literature “distorted fluorite” HP polymorph of NiF_2 (assumed $I4/mmm$) would have too high enthalpy. Instead, we propose formation of orthorhombic distorted PdF_2 type structure ($Pbca$ symmetry), which is consistent with CoF_2 and CuF_2 sequences of pressure-induced PTs.

S2. Supplementary Figures

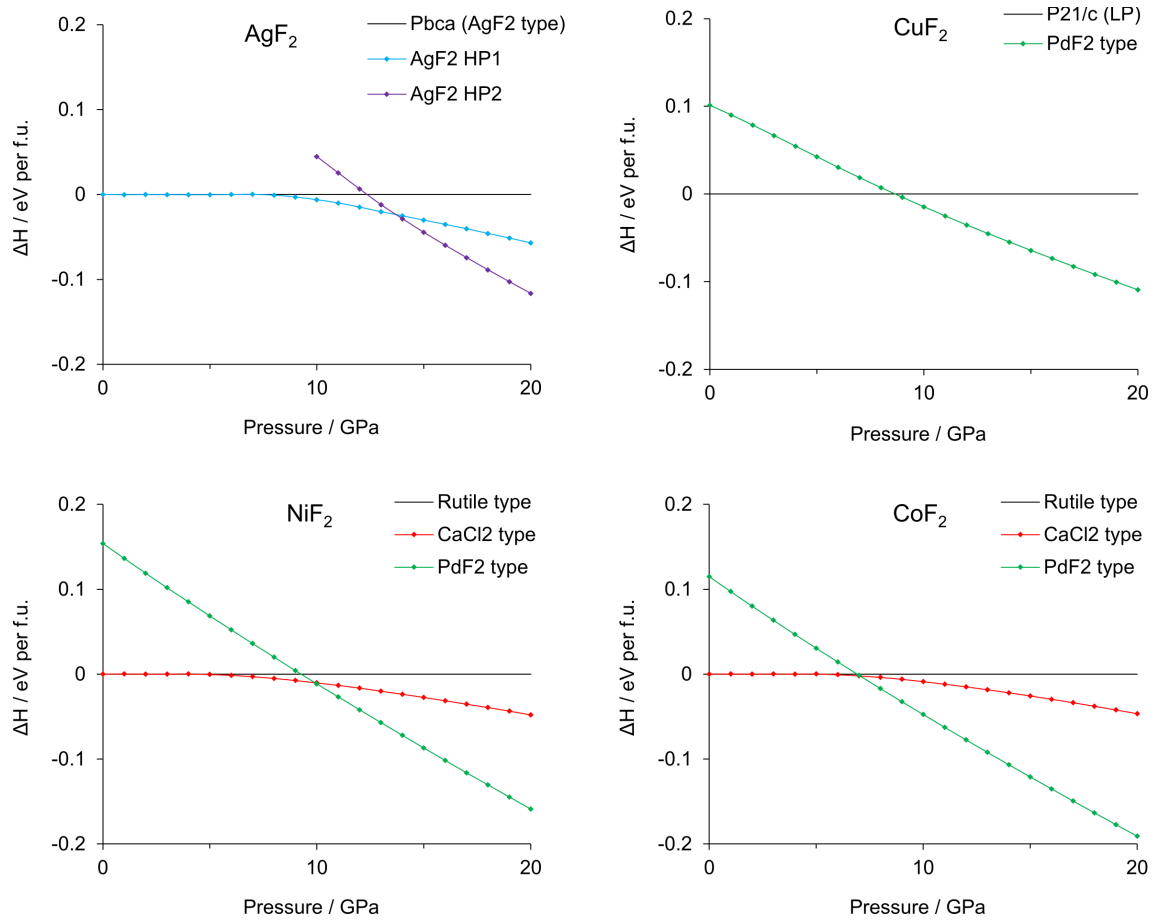


Figure S1. Enthalpy versus pressure diagrams for parent binary fluorides.

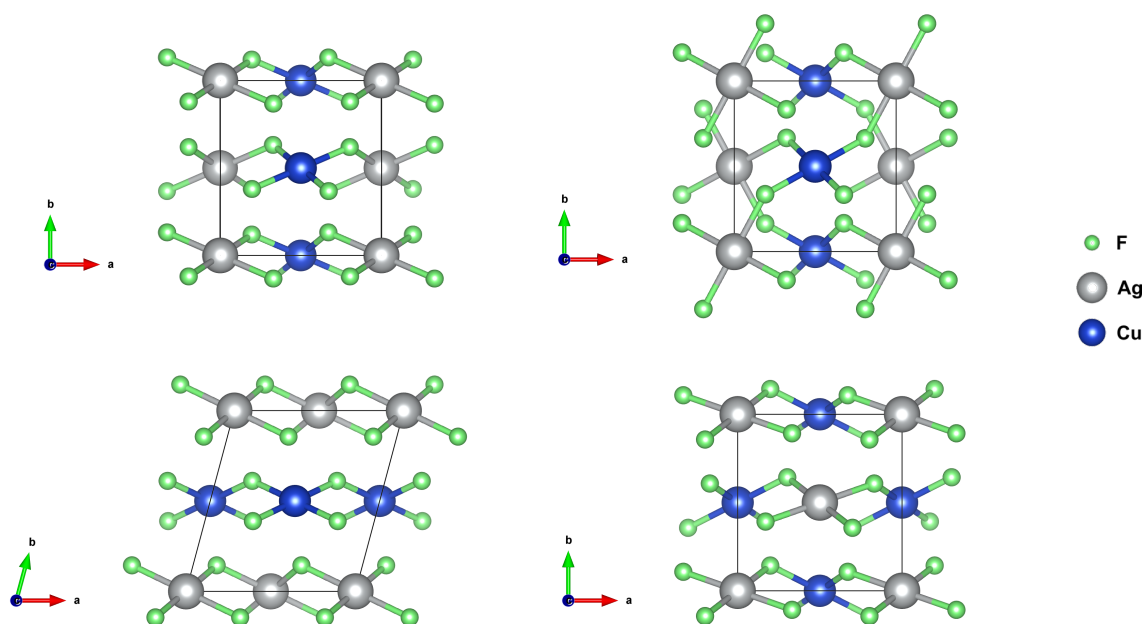


Figure S2. Structures of AgCuF_4 originating from various substitutions within AgF_2 type structure enabled by its orthorhombic symmetry. Starting from top-left corner: $\perp \vec{a}, \perp \vec{a}$ (3D, HP1 polytype), $\perp \vec{b}$ (SL, LP polytype) and $\perp \vec{c}$.

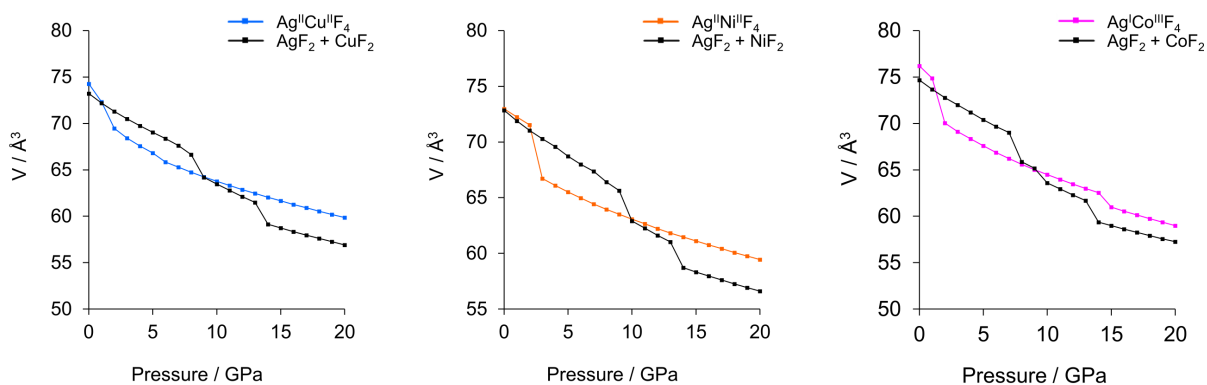


Figure S3. Pressure versus volume plots for the lowest-enthalpy polymorphs of AgCuF_4 , AgNiF_4 and AgCoF_4 with respect to the considered substrates.

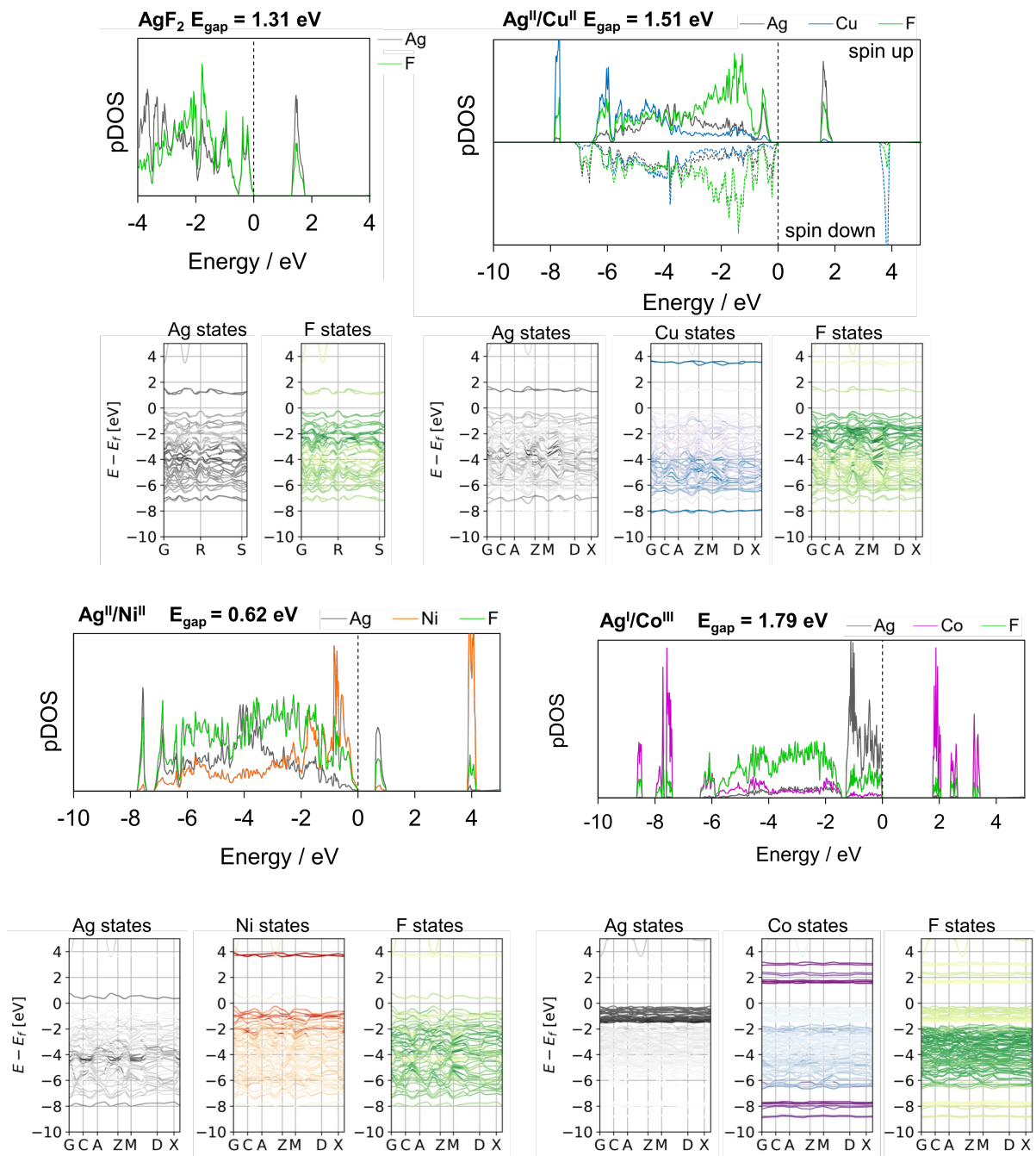


Figure S4. Electronic density of states and band structures of AgF₂, AgCuF₄, AgNiF₄ and AgCoF₄ at 10 GPa.

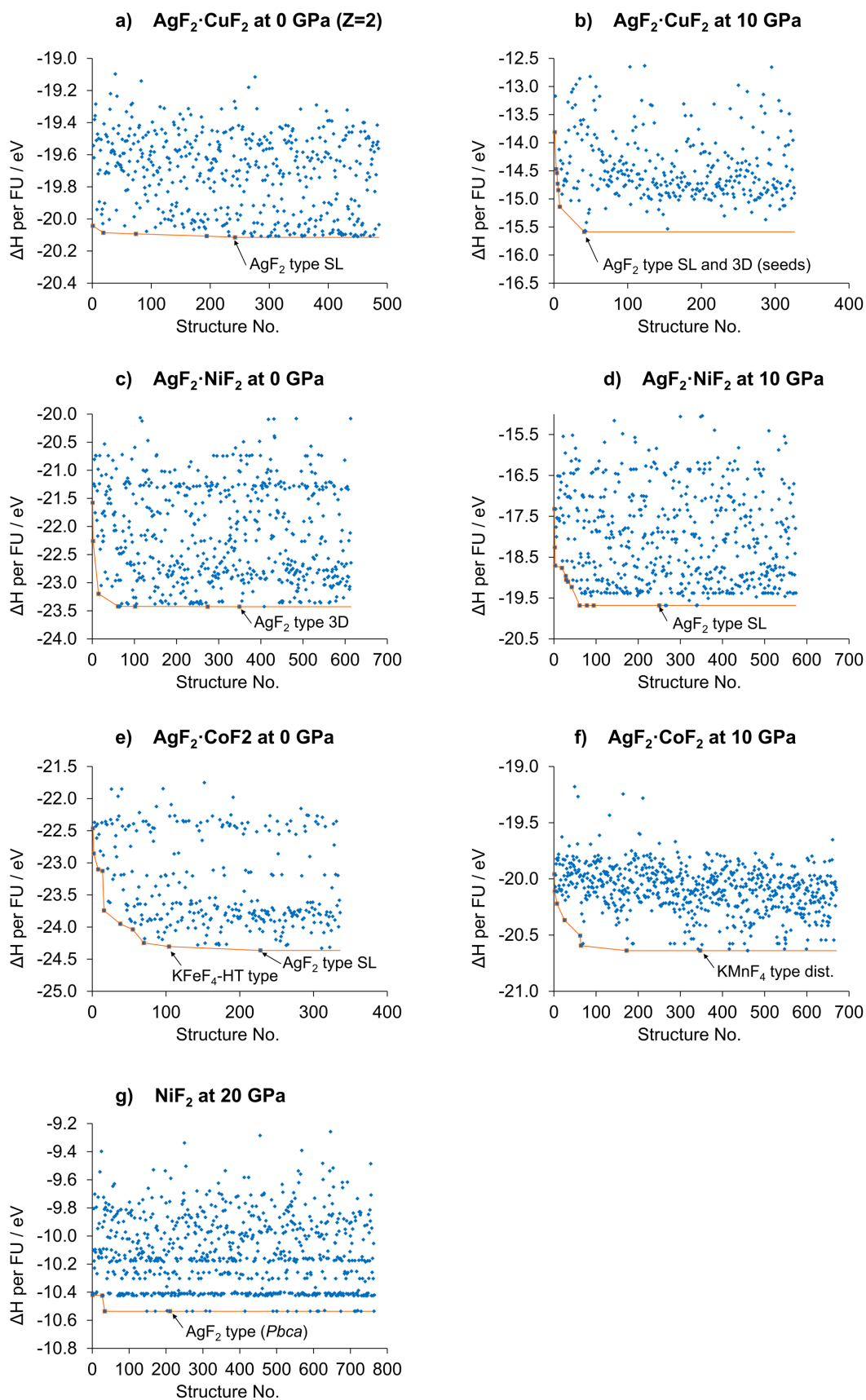


Figure S5. Performed XtalOpt quests for the lowest-enthalpy structures for the AgCuF_4 , AgNiF_4 , AgCoF_4 and NiF_2 stoichiometries for $Z=4$ (with the one exception marked for $\text{AgF}_2 \cdot \text{CuF}_2$ at 0 GPa). All structures energies are marked with blue diamonds, while the lowest-enthalpy structures are marked with orange squares and are connected with lines.

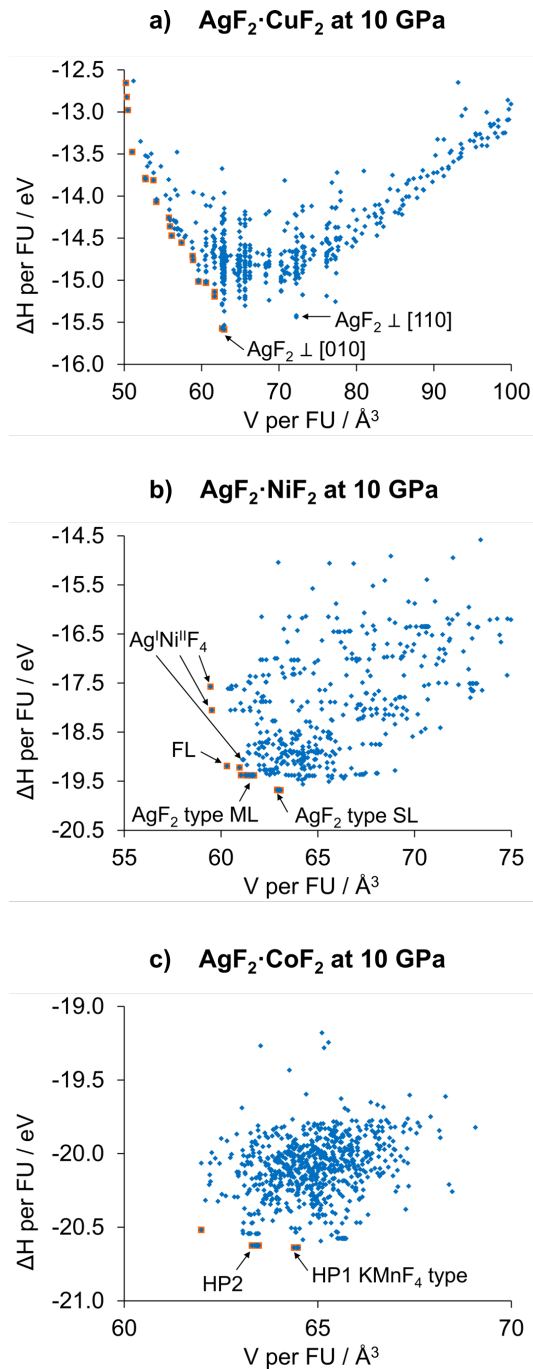


Figure S6. Performed XtalOpt quests for the lowest-enthalpy structures for the AgCuF_4 , AgNiF_4 and AgCoF_4 stoichiometries for $Z=4$ at 10 GPa. All structures energies are marked with blue diamonds, while the lowest enthalpy & volume structures are marked with orange squares. On the plot **a)** given crystal directions mark the substitution plane in particular structures. On the plot **b)** FL denotes flat layers (mixed Ag-Ni layers) polymorph, ML buckled layers (mixed Ag-Ni layers) polymorph, while SL separate layers polymorph (*i.e.* element separated).

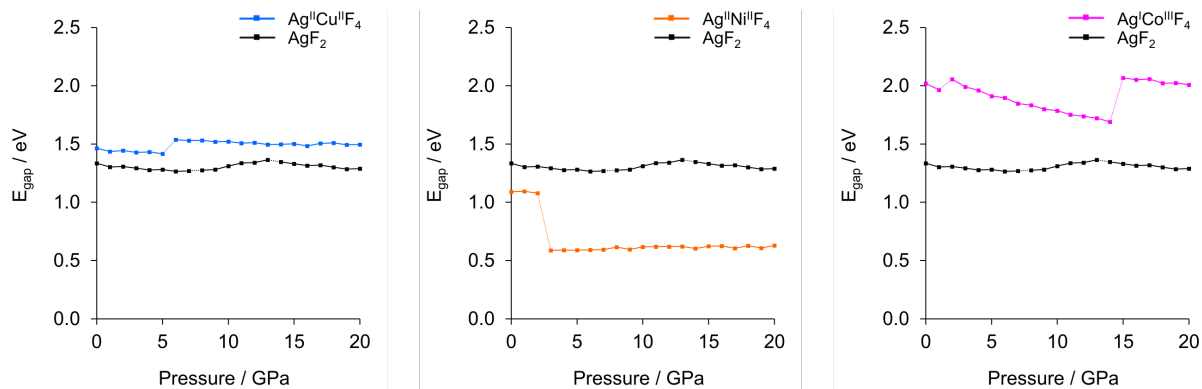


Figure S7. Electronic band gaps dependency on pressure increase for the lowest-enthalpy structures of AgCuF_4 , AgNiF_4 and AgCoF_4 (shown together with AgF_2). Dotted lines connect structures separated by corresponding phase transitions. Detailed data is provided in the **Table S3**.

S3. Supplementary Tables

Table S1. Phase transition pressures obtained from GGA+U calculations for parent binary fluorides compared with experimental data.

Substrates phase transitions < 20 GPa

AgF ₂		
PT	Calc.	Exp. [19]
I	7.3	7.8
II	13.7	14.2

CoF ₂		
PT	Calc.	Exp. [16]
I	4.0	3.6
II	7.0	8
III	9.9	12

NiF ₂		
PT	Calc.	Exp. [21]
I	4.4	4-5
II	9.9	10

CuF ₂		
PT	Calc.	Exp. [20]
I	8.6	9

*all data given in GPa

Table S2. Comparison of GGA+U and hybrid HSE06 energies of formation and volume for presented ternary fluorides and parent phases of binary fluorides.

Structure at 0 GPa			GGA+U			HSE06		
System	Structure type	Symmetry	ΔE_f / kJ/mol	V / Å ³	V_{prod}/V_{substr}	ΔE_f / kJ/mol	V / Å ³	V_{prod}/V_{substr}
AgCoF ₄	KFeF ₄ type	<i>Pnma</i>	-4.2	76.19	102.0%	-24.8	77.32	103.0%
AgNiF ₄	AgF ₂ type (3D)	<i>P2₁/c</i>	8.6	72.98	100.2%	*-37.1	73.38	99.8%
AgCuF ₄	AgF ₂ type (SL)	<i>P2₁/c</i>	6.7	74.25	101.4%	6.1	75.78	101.3%
AgF ₂	AgF ₂ type	<i>Pbca</i>	-	40.48	-	-	41.06	-
CuF ₂	CuF ₂ type	<i>P2₁/c</i>	-	32.74	-	-	33.77	-
NiF ₂	Rutile type	<i>P4/mmm</i>	-	32.37	-	-	32.46	-
CoF ₂	Rutile type	<i>P4/mmm</i>	-	34.19	-	-	34.03	-

*with respect to the AgF + CoF₃ reaction

Structure at 10 GPa			GGA+U			HSE06		
System	Structure type	Symmetry	ΔH_f / kJ/mol	V / Å ³	V_{prod}/V_{substr}	ΔH_f / kJ/mol	V / Å ³	V_{prod}/V_{substr}
AgCoF ₄	KMnF ₄ type dist.	<i>P2₁/m</i>	-12.6	64.49	101.4%	-26.4	65.39	103.0%
AgNiF ₄	AgF ₂ type (SL)	<i>P2₁/c</i>	-3.9	63.07	100.2%	-2.1	63.57	100.2%
AgCuF ₄	AgF ₂ type (3D)	<i>P2₁/c</i>	-1.9	63.78	100.5%	-3.5	64.94	100.4%
AgF ₂	AgF ₂ HP1 type	<i>Pca2₁</i>	-	35.19	-	-	35.62	-
CuF ₂	AgF ₂ type	<i>Pbca</i>	-	28.28	-	-	29.06	-
NiF ₂	AgF ₂ type	<i>Pbca</i>	-	27.73	-	-	27.83	-
CoF ₂	AgF ₂ type	<i>Pbca</i>	-	28.40	-	-	28.16	-

Table S3. Electronic band gaps dependency on pressure increase for the lowest-enthalpy structures of AgCuF₄, AgNiF₄, AgCoF₄ and AgF₂.

p / GPa	AgF ₂		AgCuF ₄		AgNiF ₄		AgCoF ₄	
	E _{gap} / eV	Structure	E _{gap} / eV	Structure	E _{gap} / eV	Structure	E _{gap} / eV	Structure
0	1.334	LP	1.463	LP (SL)	1.091	LP (3D)	2.020	LP
1	1.302	LP	1.437	LP (SL)	1.094	LP (3D)	1.965	LP
2	1.307	LP	1.444	LP (SL)	1.079	LP (3D)	2.057	HP1
3	1.293	LP	1.429	LP (SL)	0.587	HP1 (SL)	1.991	HP1
4	1.277	LP	1.433	LP (SL)	0.589	HP1 (SL)	1.961	HP1
5	1.281	LP	1.417	LP (SL)	0.590	HP1 (SL)	1.911	HP1
6	1.266	LP	1.538	HP1 (3D)	0.591	HP1 (SL)	1.898	HP1
7	1.269	LP	1.530	HP1 (3D)	0.593	HP1 (SL)	1.847	HP1
8	1.275	HP1	1.532	HP1 (3D)	0.615	HP1 (SL)	1.833	HP1
9	1.282	HP1	1.519	HP1 (3D)	0.596	HP1 (SL)	1.800	HP1
10	1.311	HP1	1.522	HP1 (3D)	0.618	HP1 (SL)	1.786	HP1
11	1.337	HP1	1.507	HP1 (3D)	0.620	HP1 (SL)	1.753	HP1
12	1.341	HP1	1.511	HP1 (3D)	0.620	HP1 (SL)	1.738	HP1
13	1.364	HP1	1.495	HP1 (3D)	0.622	HP1 (SL)	1.723	HP1
14	1.347	HP2	1.497	HP1 (3D)	0.603	HP1 (SL)	1.690	HP1
15	1.330	HP2	1.501	HP1 (3D)	0.624	HP1 (SL)	2.069	HP2
16	1.314	HP2	1.484	HP1 (3D)	0.625	HP1 (SL)	2.053	HP2
17	1.318	HP2	1.505	HP1 (3D)	0.606	HP1 (SL)	2.058	HP2
18	1.301	HP2	1.509	HP1 (3D)	0.627	HP1 (SL)	2.022	HP2
19	1.285	HP2	1.493	HP1 (3D)	0.608	HP1 (SL)	2.025	HP2
20	1.288	HP2	1.495	HP1 (3D)	0.629	HP1 (SL)	2.009	HP2

S4. Crystal structures in POSCAR format

AgCuF4 SL at 0 GPa (P2₁/c)

```
1.0000000000000000
 5.3901036487284317  0.7313930884644128  0.0000000000000000
 0.7999934734740585  5.8918165998868357  0.0000000000000000
 0.0000000000000000  0.0000000000000000  4.7638498089899999
Ag   Cu   F
 2    2    8
```

Direct

```
-0.0000000000000000 -0.0000000000000000 -0.0000000000000000
 0.5000000000000000 -0.0000000000000000  0.5000000000000000
-0.0000000000000000  0.5000000000000000  0.5000000000000000
 0.5000000000000000  0.5000000000000000 -0.0000000000000000
 0.361022220924554  0.8549158998614186  0.1646245680338823
 0.6389777799075446  0.1450840701385790  0.8353754559661197
 0.1389777799075446  0.1450840701385790  0.6646245910338806
 0.8610222630924554  0.8549158998614186  0.3353754559661197
 0.7865728171829347  0.3876784498046880  0.2457279423781989
 0.2134271828170653  0.6123215501953191  0.7542721046218013
 0.7134272258170653  0.6123215501953191  0.7457279423781991
 0.2865728171829346  0.3876784498046880  0.2542720816218031
```

AgCuF4 3D at 10 GPa (P2₁/c)

```
1.0000000000000000
 4.9274005811963182  0.0000000000000000  -0.0515194211623682
 0.0000000000000000  5.1535447840790782  0.0000000000000000
-0.0654618047501239  0.0000000000000000  5.0237402810958489
Ag   Cu   F
 2    2    8
```

Direct

```
0.0000000000000000 -0.0000000000000000 -0.0000000000000000
 0.0000000000000000  0.5000000000000000  0.5000000000000000
 0.5000000000000000  0.5000000000000000 -0.0000000000000000
 0.5000000000000000 -0.0000000000000000  0.5000000000000000
 0.3389463792717425  0.8347599318493771  0.1960332912334153
 0.6610536207282576  0.1652400381506133  0.8039667327665866
 0.1779727376733418  0.1555907884328188  0.5930914897534010
 0.8220273053266582  0.8444091815671787  0.4069085572465994
 0.6610536207282576  0.3347599718493946  0.3039667327665866
 0.3389463792717425  0.6652400281506196  0.6960333142334137
 0.8220273053266582  0.6555907784328180  0.9069085572465994
 0.1779727376733418  0.3444092215671749  0.0930914667534026
```

AgNiF4 3D at 0 GPa (P2_1/c)

1.0

5.6236634254	0.0000000000	0.0000000000
0.0000000000	4.8052668571	0.0000000000
-1.6601559382	0.0000000000	5.4010045697

Ag	Ni	F
2	2	8

Direct

0.0000000000	0.0000000000	0.0000000000
0.000000010	0.5000000000	0.500000021
0.500000000	0.500000000	0.000000000
0.500000021	-0.000000000	0.500000021
0.631682708	0.291337303	0.316754088
0.368317340	0.708662772	0.683245975
0.827889647	0.830939754	0.599213142
0.172110334	0.169060234	0.400786943
0.368316524	0.791337526	0.183244983
0.631683475	0.208662449	0.816755058
0.172111236	0.330939109	0.900784888
0.827888830	0.669060842	0.099215164

AgNiF4 SL at 10 GPa (P2_1/c)

1.0000000000000000

5.0886782073707630	0.0000000000000000	0.1368241482182605
0.0000000000000000	4.8499977824595426	0.0000000000000000
-0.8194022892055097	0.0000000000000000	5.0886650244517631

Ag	Ni	F
2	2	8

Direct

0.5000000100000008	0.0000000000000000	0.5000000000000000
0.5000000000000000	0.5000000000000000	0.0000000000000000
-0.0000000000000000	0.0000000000000000	-0.0000000000000000
0.9999999900000035	0.5000000000000000	0.5000000000000000
0.8690903136360084	0.1781934389142069	0.2948350645973958
0.1309096353639909	0.8218065730857941	0.7051649114026022
0.1309096403639878	0.6781934269142059	0.2051649344026005
0.8690903276360096	0.3218065730857941	0.7948350875973942
0.3441785184272516	0.3509922888094633	0.6260187667631506
0.6558214965727461	0.6490076871905347	0.3739812102368510
0.6558215105727473	0.8509922638094648	0.8739812322368529
0.3441785114272546	0.1490077231905305	0.1260187787631515

AgCoF4 KFeF4-LT-type at 0 GPa (Pnma)

1.0000000000000000

11.0229778442210424	0.0000000000000000	0.0000000000000000
0.0000000000000000	7.3311291705040329	0.0000000000000000
0.0000000000000000	-0.0000000000000000	7.5425856227456265

Ag	Co	F
8	8	32

Direct

0.9683188982466118	0.2500000000000000	0.1255183651661389
0.0316810847533832	0.7500000160000013	0.8744816728338642
0.9837239260802026	0.2500000000000000	0.6228451327222728
0.0162760599197891	0.7500000160000013	0.3771549282777215
0.5316811017533882	0.7500000160000013	0.6255183571661382
0.4683188982466118	0.2500000000000000	0.3744816428338617
0.5162760739197974	0.7500000160000013	0.1228450867222762
0.4837239260802098	0.2500000000000000	0.8771548982777262
0.7467105127796945	0.4990345616993822	0.3738868254660963
0.7532894872203055	0.9990345616993822	0.8738868864660977
0.7532894872203055	0.5009654383006178	0.8738868864660977
0.7467105127796945	0.0009654253006132	0.3738868254660963
0.2532895072203000	0.9990345616993822	0.6261131435339048
0.2467105127797016	0.4990345616993822	0.1261131665339031
0.2467105127797016	0.0009654253006132	0.1261131665339031
0.2532895072203000	0.5009654383006178	0.6261131435339048
0.7539609126181328	0.0535814051346022	0.1238451037124495
0.2460390493818711	0.9464186048653986	0.8761549272875495
0.7460390873818672	0.9464186048653986	0.6238451037124495
0.2539608926181312	0.0535814051346022	0.3761548962875505
0.2460390493818711	0.5535814261346075	0.8761549272875495
0.7539609126181328	0.4464185738653925	0.1238451037124495
0.2539608926181312	0.4464185738653925	0.3761548962875505
0.7460390873818672	0.5535814261346075	0.6238451037124495
0.1963206150647456	0.2500000000000000	0.0795629127220840
0.8036793849352544	0.7500000160000013	0.9204370722779112
0.3036793649352528	0.7500000160000013	0.5795628977220864
0.6963206150647456	0.2500000000000000	0.4204370722779112
0.2938130443724235	0.7500000160000013	0.1739096856442099
0.7061869556275694	0.2500000000000000	0.8260903443557925
0.2061869556275765	0.2500000000000000	0.6739096856442099
0.7938130443724306	0.7500000160000013	0.3260903143557901
0.4070914288000720	0.0605024491404656	0.1132071308650861
0.5929085711999279	0.9394975318595364	0.8867929071349100
0.0929085711999280	0.9394975318595364	0.6132071228650925
0.9070913908000761	0.0605024491404656	0.3867928771349146
0.5929085711999279	0.5605025001404662	0.8867929071349100
0.4070914288000720	0.4394975628595353	0.1132071308650861
0.9070913908000761	0.4394975628595353	0.3867928771349146
0.0929085711999280	0.5605025001404662	0.6132071228650925
0.0859978345849887	0.9426344231570277	0.1375159744150148
0.9140022044150110	0.0573655528429703	0.8624839795849886
0.4140021654150113	0.0573655528429703	0.6375159894150124
0.5859977955849890	0.9426344231570277	0.3624840105849875
0.9140022044150110	0.4426343921570288	0.8624839795849886
0.0859978345849887	0.5573655448429696	0.1375159744150148

0.5859977955849890 0.5573655448429696 0.3624840105849875
0.4140021654150113 0.4426343921570288 0.6375159894150124

AgCoF4 KMnF4-type monoclinic distorted at 10 GPa (P2_1/m)

1.0000000000000000
5.1645581604201301 -0.0000000000000000 -0.0000000000000000
-0.0000000000000000 7.1288208007760936 -0.0000000000000000
-0.2681686183553522 -0.0000000000000000 7.0060921224724524

Ag Co F
4 4 16

Direct

0.5012381913199817 0.7500003415348069 0.1765428341331357
0.4987584773613909 0.2499994627704109 0.8234548225013257
0.5381112012013892 0.7499996533152838 0.6908786788800290
0.4618853107046126 0.2500005035353399 0.3091227344654247
-0.0000080995564997 -0.000008442355662 0.4999975127345845
-0.0000136385151722 0.4999966396965198 0.0000037605234955
-0.0000053607764640 0.5000003312156946 0.4999980065919969
-0.0000158398237898 0.0000035478031278 0.0000043805271134
0.8618168068943673 0.749999387999645 0.9640632722255620
0.1381785410167011 0.2499997827395836 0.0359365976662595
0.0792269506274666 0.7500002627852215 0.5860037788829671
0.9207721279647567 0.2499998008160619 0.4139949585530782
0.8640631688274300 0.0550811181571014 0.7465654681665583
0.3048455422020692 0.9313245384715036 0.9115906634229285
0.3172011439669050 0.4282452760175758 0.5771973510137838
0.8640608187847351 0.4449219082362519 0.7465646471760112
0.6951527704141568 0.4313202880577797 0.0884028473736006
0.1359367482347910 0.5550776190818745 0.2534349664641848
0.1359326286795765 0.9449190249828796 0.2534343815857265
0.6827992686805414 0.9282422440873904 0.4228086446263350
0.6828011167966012 0.5717550420208358 0.4228025545828132
0.3048465151447165 0.5686799473612165 0.9115951781725444
0.3172010542296453 0.0717584667452880 0.5771919250978584
0.6951523036200709 0.0686742860038426 0.0884073746326691

AgCoF4 KMnF4-type monoclinic distorted at 20 GPa (C2/c)

1.0000000000000000

11.0812628404247011	0.0000000000000000	-0.0059732377468867
0.0000000000000000	4.4484920880475007	0.0000000000000000
-1.5545900041669392	0.0000000000000000	4.7871892623391794

Ag	Co	F
4	4	16

Direct

-0.0000000000000000	0.9854499414981792	-0.0000000000000000
0.5000000000000000	0.4854499414981792	-0.0000000000000000
0.0000000049999969	0.6930680766525872	0.5000000189999980
0.5000000260000022	0.1930680386525841	0.5000000189999980
0.7499826645943405	0.0891191538441723	0.2499874905508578
0.2499826645943404	0.5891191278441701	0.2499874905508578
0.7500173424056565	0.5891191278441701	0.7500125234491434
0.2500173524056575	0.0891191538441723	0.7500125234491434
0.9046789962279855	0.4494612861620155	0.7950579031525441
0.4046789542279891	0.9494613381620199	0.7950579031525441
0.9046364545787734	0.2288860483661350	0.2951229472303552
0.4046364965787698	0.7288860743661372	0.2951229472303552
0.0953635414212262	0.2288860483661350	0.7048770657696495
0.5953635514212271	0.7288860743661372	0.7048770657696495
0.0953210617720122	0.4494612861620155	0.2049421348474519
0.5953210977720151	0.9494613381620199	0.2049421348474519
0.6901823796910656	0.4408622789629895	0.3802029965247833
0.1901823796910656	0.9408622789629895	0.3802029965247833
0.6901711840959881	0.2374122220893062	0.8801913918524845
0.1901711530959890	0.7374122220893062	0.8801913918524845
0.8098288629040051	0.7374122220893062	0.1198086101475157
0.3098288409040105	0.2374122220893062	0.1198086101475157
0.8098176273089386	0.9408622789629895	0.6197970174752178
0.3098176273089385	0.4408622789629895	0.6197970174752178

NiF2 orthorhombic PdF2-type at 20 GPa (Pbca)

1.0000000000000000

4.7184679081789511	-0.0000000000000000	0.0000000000000000
0.0000000000000000	4.7140006131837016	0.0000000000000000
0.0000000000000000	0.0000000000000000	4.7425333960465874

Ni F

4 8

Direct

-0.0000000000000000	-0.0000000000000000	-0.0000000000000000
0.5000000000000000	-0.0000000000000000	0.5000000000000000
0.0000000000000000	0.5000000000000000	0.5000000000000000
0.5000000000000000	0.5000000000000000	-0.0000000000000000
0.3483211307683596	0.3482448345408198	0.3468214467687561
0.6516788462316349	0.6517551424591748	0.6531785302312455
0.1516788692316403	0.6517551424591748	0.8468214697687545
0.8483211537683651	0.3482448345408198	0.1531785532312439
0.6516788462316349	0.8482448575408252	0.1531785532312439
0.3483211307683596	0.1517551654591802	0.8468214697687545
0.8483211537683651	0.1517551654591802	0.6531785302312455
0.1516788692316403	0.8482448575408252	0.3468214467687561